JPE 19-3-17

https://doi.org/10.6113/JPE.2019.19.3.794
ISSN(Print): 1598-2092 / ISSN(Online): 2093-4718

Analytical Calculation of Air Gap Magnetic Field Distribution in Magnetic Geared Motors

Hyoseok Shi†, Noboru Niguchi*, and Katsuhiro Hirata*

†,*Department of Adaptive Machine Systems, Graduate School of Engineering, Osaka University, Osaka, Japan

Abstract

Magnetic geared motors are driven using the same operating principle as conventional synchronous motors in which a magnetic gear is embedded. The magnetic geared motor is structurally similar to a magnetic gear. However, by applying currents to the stator coil, the high-speed rotor is rotated by a magnetic field and the low-speed rotor is rotated according to the gear ratio. In this paper, the operational principle of a magnetic geared motor and the magnetic flux density in its inner and outer air gaps are described. Then the magnetic flux density in the two air gaps is used to express a method for calculating the electrical and mechanical output. Results obtained with the analytical calculation method are compared with those of the finite element analysis. Finally, a prototype is used to verify the results of the analytical calculation and FEA.

Key words: Finite element analysis, Magnetic gear, Magnetic geared motor, Space harmonics

I. INTRODUCTION

Recently, there has been a lot of research on magnetic gears that can replace mechanical gears [1]-[5]. Since mechanical gears are composed of several gear pieces, they have various problems such as a vibration, noise and efficiency reduction due to friction. On the other hand, magnetic gears have a non-contact structure as a torque transmission device using the magnetic force of permanent magnets. They have a number of advantages such as no mechanical loss and maintenance-free operation. In addition, they have inherent damage protection from overload. Accordingly, various novel structures such as vernier motors [6]-[10], continuously variable speed gears [11]-[13] and magnetic geared motors [14]-[18] have been proposed using the principles of magnetic gears. In particular, a magnetic geared motor has been developed by applying the structure of a magnetic gear and a conventional electric motor. The magnetic geared motor is composed of a high-speed rotor, a low-speed rotor and a stator like a magnetic gear [1], where the coils are wound on the stator [19]. When a rotating magnetic field is generated by three-phase currents, the high-speed rotor is rotated by the rotating magnetic field like a conventional electrical motor, and the low-speed rotor is operated according to the gear ratio based on the principle of the magnetic gear. It should be noted that the magnetic field from the coils does not directly rotate the low-speed rotor. The rotating magnetic flux due to the coils is modulated by the low-speed rotor. However, the modulated magnetic flux does not couple with the rotating magnetic flux since the number of pole pairs for each of the magnetic fluxes is different. Since magnetic geared motors are structurally similar to magnetic gears, they are operated using space harmonics created according to a combination of the number of poles of the high-speed rotor, low-speed rotor and stator.

Recently, there have been a number of studies on magnetic geared motors. Studies on the cogging torque and torque ripple of magnetic geared motors have been conducted [15], [16] and characterization according to a structural change such as an axial type has been carried out [17]. There have been various studies on high transmission torque [18], [19]. However, analytical calculation of the magnetic geared motor have not been seen and it has been performed only to analyze the operational principle and torque characteristics such as cogging torque and torque ripple. Analytical calculations of electrical machines are expeditious tools for their design and the analysis of their performance. Prior research described the analytical calculation method of the air gap magnetic field of a vernier motor with a relatively simple structure rather than a

Manuscript received Jan. 21, 2019; accepted Apr. 9, 2019
Recommended for publication by Associate Editor Byungtaek Kim.
†Corresponding Author: shi.hyoseok@ams.eng.osaka-u.ac.jp
Tel: +81-60-6879-7533, Osaka University
*Department of Adaptive Machine Systems, Graduate School of Engineering, Osaka University, Japan

magnetic geared motor [20]. In addition, a theoretical approach of a magnetic geared motor was proposed in [21]. Both studies compared various outputs with the FEM and they showed good agreements between the FEM results and the analytical results. In this paper, the torque-speed characteristics of a magnetic geared motor are analyzed by analytical calculations and compared with the results of the finite element method and a prototype model.

First, the air gap permeance by the low-speed rotor and the magnetomotive force due to the high-speed rotor permanent magnet are described to calculate the magnetic flux density in the inner air gap. Secondly, in order to compute the magnetic flux density in the outer air gap, the primary magnetic flux density by both the low-speed rotor and the permanent magnet on the stator, and the magnetic flux density by both the high-speed rotor permanent magnet and the stator teeth are expressed. Thirdly, the back EMF and the output torque, when a current is applied, are developed using the harmonics of the previously calculated magnetic flux density. Finally, the magnetic field distributions and space harmonics in the inner and outer air gaps calculated by analytical calculation are compared with those obtained by the 2-D finite element method. In addition, the outputs of the electromotive force and torque are verified by carrying out measurements on a prototype model.

II. Analytical Calculation of the Air Gap Magnetic Flux Density Distribution in a Magnetic Geared Motor

The magnetic-geared motor shown in Fig. 1 is based on the structure of a magnetic gear, which consists of high-speed and low-speed rotors and a stator. The high-speed rotor is composed of a yoke and the 5 pole pairs of a permanent magnet (Br=1.44T). The low-speed rotor consists of 17 magnetic pole pieces formed by laminated steel sheets 50A400. The 12 slot stator has a three-phase concentrated winding. The high-speed rotor is rotated by current applied to the coil wound on the stator with a winding factor of 0.933. It should be stressed here that the low-speed rotor cannot be rotated by the rotating flux due to the current. The low-speed rotor is rotated by employing the operational principle of a magnetic gear. In other words, N_h, N_l and N_s must satisfy the following equation [19]:

$$N_s = (2n-1)N_l \mp (2\,\mathrm{m}-1)N_h \quad (1)$$

where m and n are positive integers, N_h is the pole-pair number of the permanent magnet on the high-speed rotor, N_l is the number of steel pole pieces in the low speed rotor, and N_s is the number of slots and pole pairs of the permanent magnet in the stator.

To analytically calculate the air gap magnetic fields of the magnetic geared motor, the magnetic flux densities of the outer and inner air gaps should be separately calculated centering on the low-speed rotor.

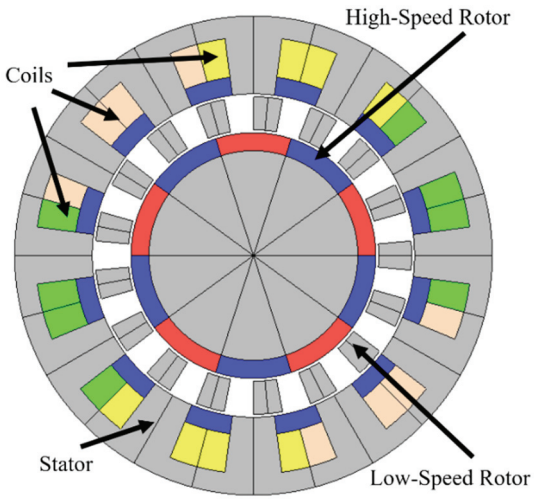

Fig. 1. Cross Section of a magnetic geared motor.

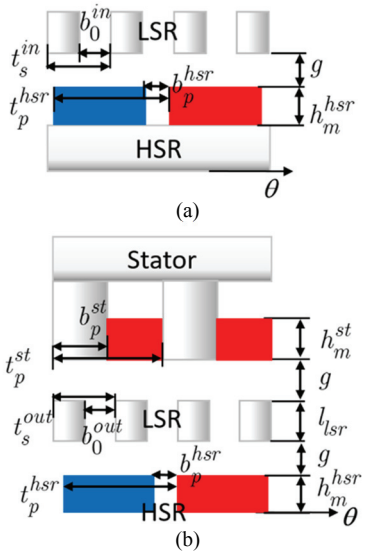

(a)

(b)

Fig. 2. Slotted structure. (a) Inner air gap without a stator. (b) Overall structure.

A. Magnetic Flux Density in the Inner Air Gap

In order to calculate the magnetic flux density distribution in the inner air gap, it is assumed that there is no stator. Only the high-speed rotor and low-speed rotor are used for the calculation. This is because the magnetomotive force generated by the permanent magnet on the stator has a considerably small influence on the inner air gap. An analytical method for modeling the effect of the stator slotting of a radial field brushless permanent magnet dc motor was presented in [23]. The air gap permeance of the low-speed rotor teeth with the slotting effect, as shown in Fig. 2(a), can be calculated by a Fourier decomposition with a unit magnetic potential between the low-speed rotor teeth and the high-speed rotor magnet. Therefore, the permeance function $P^{in}(\theta+\delta)$ of the low-speed rotor can be described by the following equation:

$$P^{in}(\theta+\delta)=P_0^{in}+\sum_{i=1}^{\infty}P_i^{in}\cos\left\{(2i-1)N_l(\theta+\delta)\right\} \quad (2)$$

where N_l is the number of the low-speed rotor pole pieces. The coefficients P_0^{in} and P_i^{in} in (2) can be obtained as follows:

$$P_0^{in}=\frac{\mu_0}{K_c^{in}g_e^{in}}\left(1-1.6\beta^{in}r_o^{in}\right) \quad (3)$$

$$g_e^{in}=g+\frac{h_m^{hsr}}{\mu_r} \quad (4)$$

$$P_i^{in}=\frac{4}{i\pi}\frac{\mu_0}{g_e^{in}}\beta^{in}\left[0.5+\frac{\left(ir_o^{in}\right)^2}{0.78125-2\left(ir_o^{in}\right)^2}\right]\sin\left(1.6\pi ir_o^{in}\right) \quad (5)$$

$$K_c^{in}=\left[1-\frac{2}{\pi}r_o^{in}\left\{\tan^{-1}\left(\frac{b_0^{in}}{g_e^{in}}\right)-\frac{g_e^{in}}{b_0^{in}}\ln\left[1+\frac{1}{4}\left(\frac{b_0^{in}}{g_e^{in}}\right)\right]\right\}\right]^{-1} \quad (6)$$

$$\beta^{in}=\frac{1}{2}+\frac{1}{2\sqrt{1+\left(\frac{t_s^{in}r_o^{in}}{2g_e^{in}}\right)}} \quad (7)$$

where r_o^{in} is the opening ratio of the opening length b_0^{in} to the pitch t_s^{in}; μ_r and μ_0 are the relative permeabilities of the low-speed rotor and the high speed yokes with respect to the permeability of vacuum. g, h_m^{hsr} and g_e^{in} are the air gap length, the permanent magnet thickness shown in Fig. 2(a), and the replaced air gap length for the computation of Carter's coefficient [22]. The Carter's coefficient K_c^{in} has been included to account for the increase in the effective air gap length due to the slotting phenomenon of the low-speed rotor. The magnetomotive force due to the permanent magnet of the high-speed rotor is expressed by [21]:

$$F^{hsr}(\theta+\gamma)=\sum_{j=1}^{\infty}A_j^{hsr}\cos\left\{(2j-1)N_h(\theta+\gamma)\right\} \quad (8)$$

where N_h is the pole-pair number of the permanent magnet of the high-speed rotor. The coefficient A_j^{hsr} of the MMF function is the magnetization, which is assumed to be uniform throughout the cross-section of the permanent magnets and is given by [23]:

$$A_j^{hsr}=\frac{B_r}{\mu_0 jN_h}r_p^{hsr}h_m^{hsr}\frac{\sin\left(\frac{j\pi r_p^{hsr}}{2}\right)}{\frac{j\pi r_p^{hsr}}{2}} \quad (9)$$

where B_r is the permanent magnet remanence, and r_p^{hsr} is the ratio of the permanent magnet pole $\left(t_p^{hsr}-b_p^{hsr}\right)$ to the pole pitch t_p^{hsr}. Using the product between the air gap permeance $P^{in}(\theta+\delta)$ and the magnetomotive force $F^{hsr}(\theta+\gamma)$, the magnetic flux density in the inner air gap can be obtained by (10).

B. Magnetic Flux Density in the Outer Air Gap

To calculate the magnetic field distribution in the outer air gap, it is necessary to compute the magnetic flux density by the magnetomotive force of the permanent magnet between the stator teeth and the air gap permeance by the low-speed rotor. It is also necessary to consider the influence of the permanent magnet on the high-speed rotor. Thus, the magnetic flux density in the outer air gap can be described as a combination of the magnetic flux from the magnetomotive force due to the permanent magnet and permeance of the low-speed rotor, and the magnetomotive force due to the permanent magnet on the stator teeth and the air gap permeance of the low-speed rotor. As mentioned above, the methods used for calculating the air gap permeance and magnetomotive force are similar to those discussed above. The outer air gap permeance $P^{out}(\theta+\delta)$ of the low-speed rotor can be obtained as follow:

$$P^{out}(\theta+\delta)=P_0^{out}+\sum_{i=1}^{\infty}P_i^{out}\cos\left\{(2i-1)N_l(\theta+\delta)\right\} \quad (11)$$

$$P_0^{out}=\frac{\mu_0}{K_c^{out}g_e^{out}}\left(1-1.6\beta^{out}r_o^{out}\right) \quad (12)$$

$$g_e^{out}=g+\frac{h_m^{st}}{\mu_r} \quad (13)$$

$$P_i^{out}=\frac{4}{i\pi}\frac{\mu_0}{g_e^{out}}\beta^{out}\left[0.5+\frac{\left(ir_o^{out}\right)^2}{0.78125-2\left(ir_o^{out}\right)^2}\right]\sin\left(1.6\pi ir_o^{out}\right) \quad (14)$$

$$\begin{aligned}B^{inner}(\theta)&=F^{hsr}(\theta+\gamma)P^{in}(\theta+\delta)\\&=\sum_{j=1}^{\infty}A_j^{hsr}P_0^{in}\cos\left\{(2j-1)N_h(\theta+\gamma)\right\}\\&+\sum_{i=1}^{\infty}\sum_{j=1}^{\infty}\frac{A_j^{hsr}P_i^{in}}{2}\times\left[\begin{array}{l}\cos\left[\left\{(2j-1)N_h+(2i-1)N_l\right\}\left\{\theta+\frac{(2j-1)N_h\gamma+(2i-1)N_l\delta}{(2j-1)N_h+(2i-1)N_l}\right\}\right]\\+\cos\left[\left\{(2j-1)N_h-(2i-1)N_l\right\}\left\{\theta+\frac{(2j-1)N_h\gamma-(2i-1)N_l\delta}{(2j-1)N_h-(2i-1)N_l}\right\}\right]\end{array}\right]\end{aligned} \quad (10)$$

$$K_c^{out} = \left[1-\frac{2}{\pi}r_o^{st}\left\{\tan^{-1}\left(\frac{b_0^{st}}{g_e^{out}}\right)-\frac{g_e^{out}}{b_0^{st}}\ln\left[1+\frac{1}{4}\left(\frac{b_0^{st}}{g_e^{out}}\right)\right]\right\}\right]^{-1} \quad (15)$$

$$\beta^{out} = \frac{1}{2}+\frac{1}{2\sqrt{1+\left(\frac{t_s^{st}r_o^{out}}{2g_e^{out}}\right)}} \quad (16)$$

where r_o^{out} is the ratio of the opening length b_0^{out} to the pitch t_s^{out} of the low-speed rotor adjacent to the outer air gap, and h_m^{st} is the permanent magnet thickness as shown in Fig. 2(b). In (15), K_t^{out} is the Carter's coefficient, and g_e^{out} is the replaced air gap length for the computation of the Carter's coefficient of the outer air gap.

The magnetomotive force of the permanent magnet on the stator is expressed by:

$$F^{st}(\theta) = \sum_{l=1}^{\infty} A_l^{st}\cos\left\{(2l-1)N_s\theta\right\} \quad (17)$$

$$A_l^{st} = \frac{B_r}{\mu_0 l N_s}r_p^{st}h_m^{st}\frac{\sin\left(\frac{l\pi r_p^{st}}{2}\right)}{\frac{l\pi r_p^{st}}{2}} \quad (18)$$

where r_0^{st} is the ratio of the permanent magnet length to the stator pitch, which is 0.5 in this model. N_s is the number of the stator teeth, and h_m^{st} is the thickness of the permanent magnet on the stator teeth.

To express the influence of the permanent magnet on the high-speed rotor, the magnetic field is obtained by the product between the air gap permeance by the stator teeth and the magnetomotive force by the high-speed rotor magnet. Therefore, the air gap permeance function $P^{st}(\theta)$ of the stator teeth can be obtained by (19).

$$P^{st}(\theta) = P_0^{st}+\sum_{k=1}^{\infty}P_k^{st}\cos\left\{(2k-1)N_s\theta\right\} \quad (19)$$

$$P_0^{st} = \frac{\mu_0}{K_c^{st}g_e^{st}}\left(1-1.6\beta^{st}r_o^{st}\right) \quad (20)$$

$$g_e^{st} = 2g+l_{lsr}+\frac{h_m^{st}}{\mu_r} \quad (21)$$

$$P_k^{st} = \frac{4}{k\pi}\frac{\mu_0}{g_e^{out}}\beta^{st}\left[0.5+\frac{\left(ir_o^{st}\right)^2}{0.78125-2\left(ir_o^{st}\right)^2}\right]\sin\left(1.6\pi ir_o^{st}\right) \quad (22)$$

$$K_c^{st} = \left[1-\frac{2}{\pi}r_o^{st}\left\{\tan^{-1}\left(\frac{b_0^{st}}{g_e^{st}}\right)-\frac{g_e^{st}}{b_0^{st}}\ln\left[1+\frac{1}{4}\left(\frac{b_0^{st}}{g_e^{st}}\right)\right]\right\}\right]^{-1} \quad (23)$$

$$\beta^{st} = \frac{1}{2}+\frac{1}{2\sqrt{1+\left(\frac{t_s^{st}r_o^{st}}{2g_e^{st}}\right)}} \quad (24)$$

where g_e^{st} is the effective air gap length obtained as the sum of the inner and outer air gaps and the length of the low-speed rotor. Other coefficients are calculated by applying the stator teeth in the process described above. Finally, the magnetic flux density in the outer air gap can be obtained as the sum of the products between the magnetomotive force due to the permanent magnet and the air gap permeance of the low-speed rotor teeth, and between the magnetomotive force of the high-speed rotor magnet and the air gap permeance of the stator teeth as (25).

C. Back EMF and Torque

In the case of a three-phase surface permanent synchronous motor, the general torque equation is as follows:

$$T_e = \frac{P}{\omega_m} = \frac{e_u i_u + e_v i_v + e_w i_w}{\omega_m} \quad (26)$$

$$\begin{aligned}
B^{outer}(\theta,\delta,\gamma) &= F^{st}(\theta)P^{out}(\theta+\delta)+F^{hsr}(\theta+\gamma)P^{st}(\theta)\\
&= \sum_{l=1}^{\infty}A_l^{st}P_0^{out}\cos\left\{(2l-1)N_s\theta\right\}+\sum_{j=1}^{\infty}A_j^{hsr}P_0^{st}\cos\left\{(2j-1)N_h(\theta+\gamma)\right\}\\
&+\sum_{l=1}^{\infty}\sum_{i=1}^{\infty}\frac{A_l^{st}P_i^{out}}{2}\times\left[\begin{array}{l}\cos\left[\left\{(2l-1)N_s+(2i-1)N_l\right\}\left\{\theta+\frac{(2i-1)N_l\delta}{(2l-1)N_s+(2i-1)N_l}\right\}\right]\\+\cos\left[\left\{(2l-1)N_s-(2i-1)N_l\right\}\left\{\theta+\frac{(2i-1)N_l\delta}{(2l-1)N_s-(2i-1)N_l}\right\}\right]\end{array}\right]\\
&+\sum_{j=1}^{\infty}\sum_{k=1}^{\infty}\frac{A_j^{hsr}P_k^{st}}{2}\times\left[\begin{array}{l}\cos\left[\left\{(2j-1)N_h+(2k-1)N_s\right\}\left\{\theta+\frac{(2j-1)N_h\gamma}{(2j-1)N_h+(2k-1)N_s}\right\}\right]\\+\cos\left[\left\{(2j-1)N_h-(2k-1)N_s\right\}\left\{\theta+\frac{(2j-1)N_h\gamma}{(2j-1)N_h-(2k-1)N_s}\right\}\right]\end{array}\right]
\end{aligned} \quad (25)$$

where P is the power, ω_m is the rotor speed in *rad/s*, and e and i are the back electromotive force (EMF) and current of each phase, respectively.

For a conventional surface permanent magnet synchronous motor, the back EMF is the derivate of the flux linkage waveform. However, since magnetic geared motors have a geared effect, they contain a coefficient k_r when calculating the back EMF. The phase back EMF of a magnetic geared motor can be obtained by:

$$e_{ph} = \frac{d\lambda}{dt} = \frac{d\theta_m}{dt}\frac{d\lambda}{d\theta_m} = k_r \omega_m \frac{d\lambda}{d\theta_m} \tag{27}$$

$$k_r = k_{hsr}^{lsr} \cdot k_{stator}^{lsr} \tag{28}$$

$$k_{lsr}^{hsr} = \frac{N_l}{N_h} \tag{29}$$

$$k_{stator}^{lsr} = \frac{N_l}{N_s} \tag{30}$$

where k_{lsr}^{hsr} and k_{stator}^{lsr} are the ratio of the number of the low-speed and high-speed rotor poles, and the ratio of the number of the low-speed rotor poles and the stator teeth. Therefore, the back EMF of a magnetic geared motor can be redefined by:

$$\begin{aligned} e_{ph} &= \frac{d\lambda}{dt} = \frac{d\theta_m}{dt}\frac{d\lambda}{d\theta_m} = k_r k_w \omega_m \frac{d\lambda}{d\theta_m} \\ &= k_r k_w \frac{N_h}{2} \omega_m \frac{2N\phi}{\pi} \\ &\approx k_r k_w \frac{N_h}{2} \omega_m \frac{2N}{\pi}\left(\frac{2\pi}{N_h} B_{g1} L_{stk} R_{ro}\right) \\ &\approx 2 k_r k_w \omega_m N B_{g1} L_{stk} R_{ro} \end{aligned} \tag{31}$$

where θ_m is the mechanical angle, k_w is the winding factor, L_{stk} is the stack length, R_{ro} is the outer radius of the low-speed rotor, and ϕ and B_{g1} are the harmonic flux and the amplitude of the 5th harmonics of the magnetic flux density in the outer air gap, respectively. Finally, the torque equation can be obtained by:

$$T_e = \frac{3}{2}\frac{e_{ph} i_{ph}}{\omega_m} \approx 3 k_r k_w N B_{g1} L_{stk} R_{ro} i_{ph} \tag{32}$$

III. FEM Verification

The 2-D finite element method was used to compare the magnetic flux density in the inner and outer air gap with the analytical calculation. To compare the results of the 2-D FEM and the analytical calculation, a magnetic geared motor was designed with the same dimensions and the parameters are listed in Table I. In the FEM analysis, a JMAG Designer 17.1.01za (JSOL Corporation) was used, and the N-T characteristics were obtained through a coupled analysis of MATLAB 7.5.0.342 (R2007b) and JMAG. A control block diagram and the analysis conditions are shown in Fig. 4 and Table II. A mesh model of a magnetic geared motor is shown in Fig. 3. The number of nodes and elements are 21,265 and 32,422, respectively. In this section, the magnetic flux density and the space harmonics distribution in the inner and outer air gaps are shown and compared through the result of the 2-D FEM and analytical calculation.

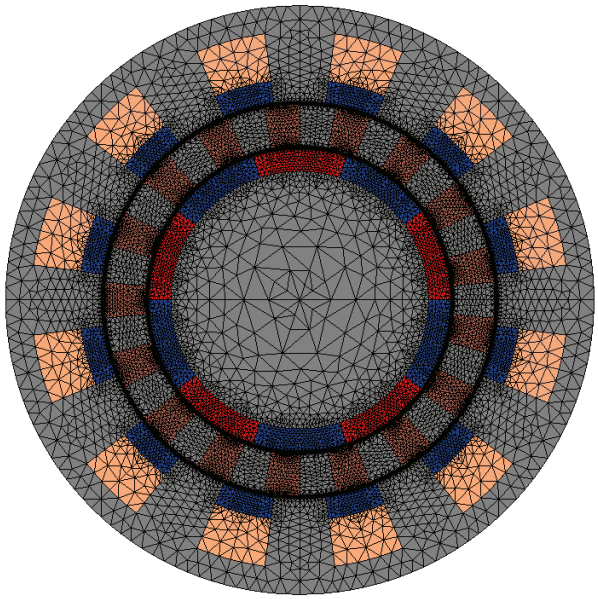

Fig. 3. Mesh model of a magnetic geared motor.

TABLE I
Main Design Parameters

Item	Unit	Value
N_h		5
N_l		17
N_s		12
Gear ratio		3.4
Stator outside radius	[mm]	R40
Stator inside radius	[mm]	R27
Low-speed rotor length	[mm]	5.5
High-speed rotor outside radius	[mm]	R20.5
Magnet thickness	[mm]	3
Stack length	[mm]	30
Air gap length	[mm]	0.5
Slot opening ratio		0.5
Magnet material		N42SH
Steel sheet		50A400

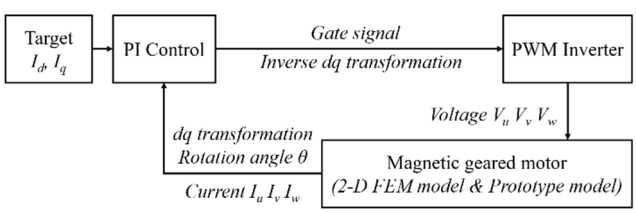

Fig. 4. Control block diagram.

TABLE II
ANALYSIS CONDITIONS

Item	Value
Carrier frequency	20kHz
Control period	2μs
Time step	2μs
Target I_d	0A
Power supply	12V

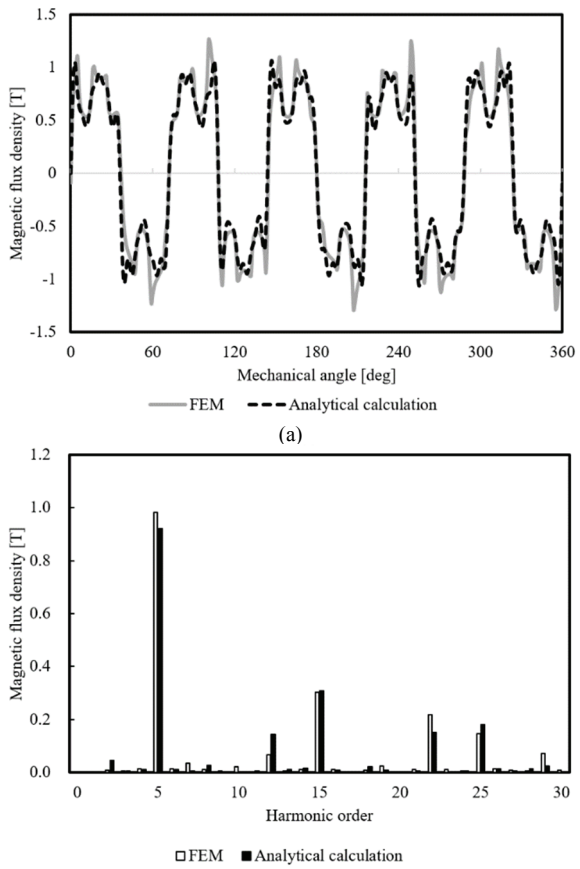

Fig. 5. Comparison of the FEM and analytical calculations in the inner air gap flux density waveform and space harmonics. (a) Flux waveform. (b) Space harmonics.

The magnetic flux density and the space harmonics distribution in the inner air gap at $t = 0$ are shown in Fig. 5. It can be seen that the analytical calculation method shows good agreement with the 2-D FEM.

Fig. 6(a) shows a comparison of the magnetic flux density in the outer air gap between analytical calculation and the 2-D FEM. In Fig. 6(a), there is a slight difference between these results. This is due to the fact that the influence of the permeability of the low-speed rotor is not reflected in the calculation of the outer gap. However, it can be seen from Fig. 6(b) that the amplitudes of the major 5th and 12th order harmonics used to drive the magnetic geared motor are very similar. This is demonstrated through analysis calculations

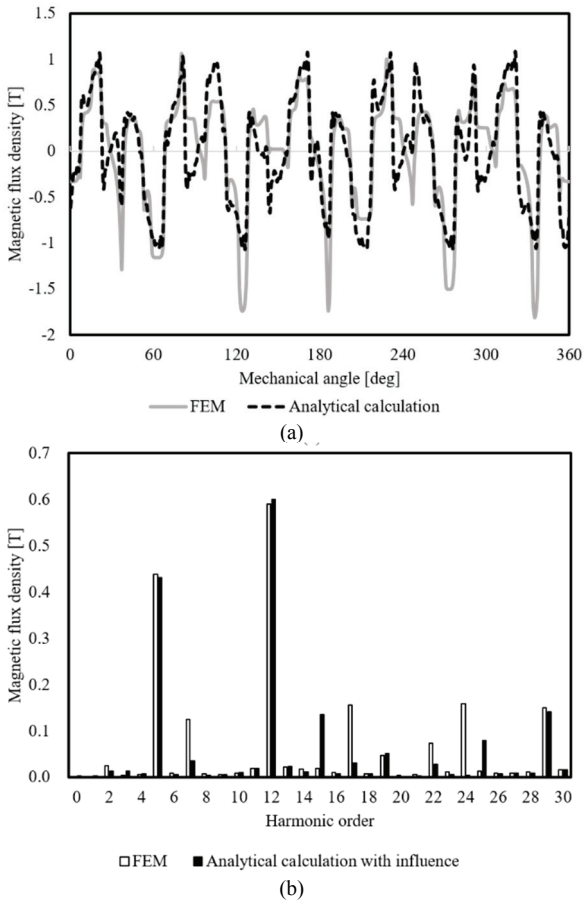

Fig. 6. Comparison of the FEM and analytical calculations in the outer air gap flux density waveform and space harmonics. (a) Flux waveform. (b) Space harmonics.

that reflect the high-speed rotor permanent magnet and the air gap permeability of the stator teeth. To obtain more accurate results, it can be estimated that the effect of the permeability of the low-speed rotor teeth should be used in analyzing the influence of the high-speed rotor permanent magnet.

IV. PROTOTYPE MODEL

In order to validate the analytical calculation, a prototype of a magnetic geared motor has been manufactured as shown in Fig. 7. The prototype was designed based on the dimensions in Table I. In the driving test, the maximum transmission torque and the back EMF were measured. Then the N-T characteristics were analyzed by driving the motor under load. Like the coupled analysis, the prototype was tested based on the control block shown in Fig. 4 and Table II. Finally, the measured results were compared and evaluated with the FEM and analytical calculation.

EMF waveforms were computed and measured when the low-speed rotor was rotated at a speed of 500rpm. The results of the back-EMF were compared among the analytical calculation, the measured prototype and the FEM as shown in Fig. 8. It can be seen that the predicted-FEM and the analytical

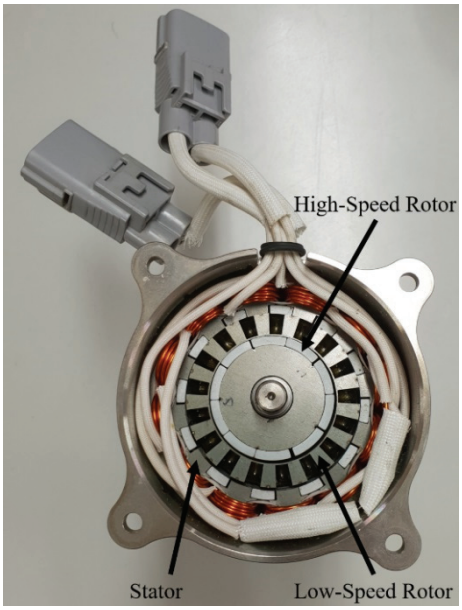

Fig. 7. Prototype of a magnetic geared motor.

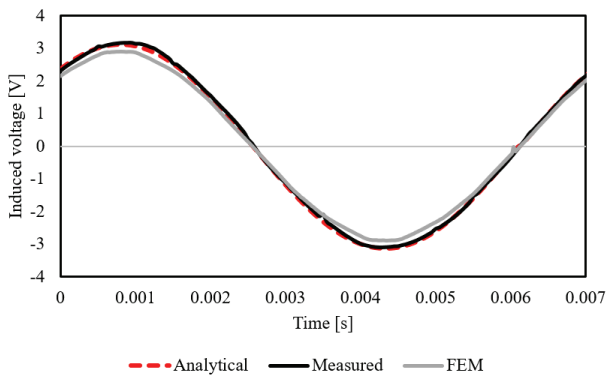

Fig. 8. Comparison of the phase back-EMF among the analytical calculation, the measured prototype and the FEM.

calculation results show a slight discrepancy from the measured results.

Fig. 9 shows a comparison of the maximum transmission torque of the FEM and the prototype when the high-speed rotor was rotated with the low-speed rotor fixed. The maximum transmission torques of the FEM and the prototype are 2.286Nm and 1.937Nm in the high-speed rotor, and 7.546Nm and 6.692Nm in the low-speed rotor, respectively. Both of these results were lower than the FEM and distorted. It is considered that a measurement error causes the brake of the slip on the low-speed rotor during measurement. Fig. 10 shows a comparison of the torque versus the speed curves of the experiments, the FEM and the analytical calculation. A good agreement can be seen between the measured and the analytical approaches. However, the FEM results show a significant difference in the range of 2 Nm to 3 Nm when compared to the analytical result. This is considered to be a computational error caused by ignoring the iron losses such as the eddy current when calculating in the FEM.

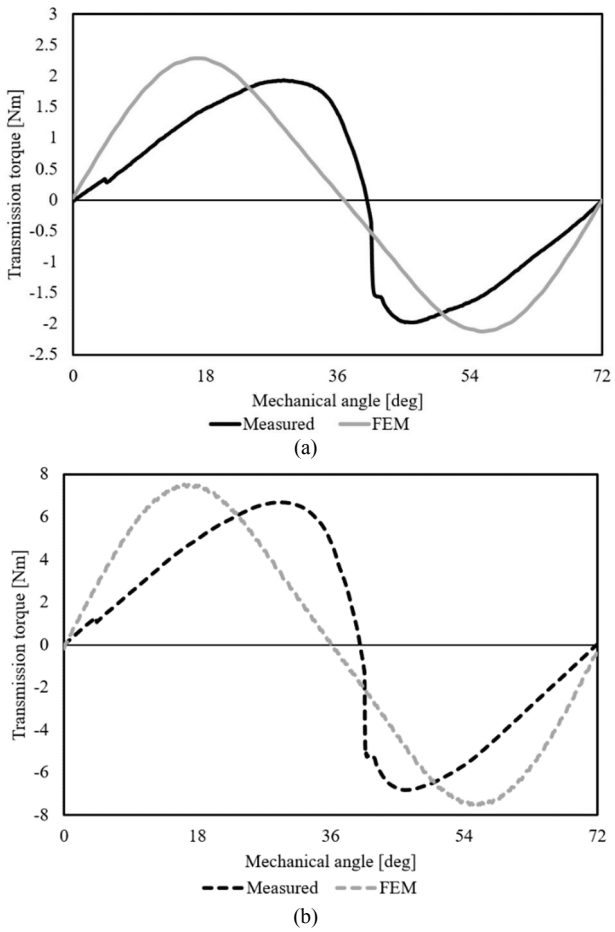

Fig. 9. Comparison of the maximum transmission torque between the FEM and the measured prototype. (a) High-speed rotor. (b) Low-speed rotor.

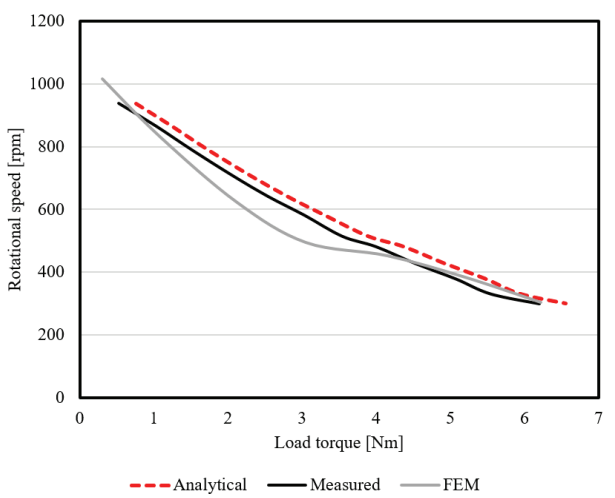

Fig. 10. Comparison of the N-T characteristics among the analytical calculation, the measured prototype and the FEM.

V. Conclusion

This paper expressed an analytical calculation that can be used to effectively and quickly analyze the N-T characteristics

of a magnetic geared motor. Results such as a magnetic flux density in the inner and outer air gap, the back-EMF and the N-T characteristics were verified and compared with the FEM and experiment on a prototype model. The analytical calculation method showed good agreement with both the FEM results and the experimental results obtained from the prototype model. In future work, an efficient design method by searching for the optimal design parameters using this calculation method will be proposed.

REFERENCES

[1] K. Atallah, and D. Howe, "A novel high-performance magnetic gear," *IEEE Trans. Magn.*, Vol. 37, No. 4, pp. 2844-2846, Jul. 2001.

[2] H. Cheng-Chi, T. Mi-Ching, D. G. Dorrell, and L. Bor-Jeng, "Development of a magnetic planetary gearbox," *IEEE Trans. Magn.*, Vol. 44, No. 3, pp. 403-412, Mar. 2008.

[3] N. Niguchi, K. Hirata, M. Muramatsu, and Y. Hayakawa, "Transmission torque characteristics in a magnetic gear," in *2010 XIX International Conference on Electrical Machines (ICEM)*, pp. 1-6, 2010.

[4] Y. Chen, W. N. Fu, S. L. Ho, and H. Liu, "A quantitative comparison analysis of radial-flux, transverse-flux, and axial-flux magnetic gears," *IEEE Trans. Magn.*, Vol. 50, No. 11, pp. 1-4, Nov. 2014.

[5] X. Zhang, X. Liu, and Z. Chen, "A novel dual-flux-modulator coaxial magnetic gear for high torque capability," *IEEE Trans. Energy Convers.*, Vol. 33, No. 2, pp. 682-691, Jun. 2018.

[6] Q. Ronghai, L. Dawei, and W. Jin, "Relationship between magnetic gears and vernier machines," in *2011 International Conference on Electrical Machines and Systems (ICEMS)*, pp. 1-6, 2011.

[7] S. Kazuhiro, R. Hosoya, and S. Shimomura, "Design of NdFeB bond magnets for in-wheel permanent magnet vernier machine," in *2012 15th International Conference on Electrical Machines and Systems (ICEMS)*, pp. 1-6, 2012.

[8] K. Byungtaek and T. A. Lipo, "Operation and design principles of a PM vernier motor," *IEEE Trans. Ind. Appl.*, Vol. 50, pp. 3656-3663, Nov. 2014.

[9] S. Hyoseok, N. Niguchi, and K. Hirata, "Characteristic analysis of surface permanent-magnet vernier motor according to pole ratio and winding pole number," *IEEE Trans. Magn.*, Vol. 53, No. 11, Nov. 2017.

[10] D. Li, T. Zou, R. Qu, and D. Jiang, "Analysis of fractional-slot concentrated winding pm vernier machines with regular open-slot stators," *IEEE Trans. Ind. Appl.*, Vol. 54, pp. 1320-1330, Mar. 2018.

[11] K. Atallah, W. Jiabin, S. D. Calverley, and S. Duggan, "Design and operation of a magnetic continuously variable transmission," *IEEE Trans. Ind. Appl.*, Vol. 48, pp. 1288-1295, Jul. 2012.

[12] A. Zaini, N. Niguchi, and K. Hirata, "Continuously variable speed vernier magnetic gear," *IEEE Trans. Magn.*, Vol. 48, pp. 3104-3107, Nov. 2012.

[13] L. Yulong, S. L. Ho, and W. N. Fu, "Novel electrical continuously variable transmission system and its numerical model," *IEEE Trans. Magn.*, Vol. 50, No. 2, pp. 757-760, Feb. 2014.

[14] J. Linni, G. Wensheng, X. Guoqing, L. Jianing, and Z. Wenxiang, "Integrated magnetic-geared machine with sandwiched armature stator for low-speed large-torque applications," *IEEE Trans. Magn.*, Vol. 48, No. 11, pp. 4184-4187, Nov. 2012.

[15] N. Niguchi and K. Hirata, "Cogging torque characteristics of magnetic-geared motor," *COMPEL - The Int. J. Comput. Mathematics in Electr. Electron. Eng.*, Vol. 31, pp. 1470-1481, 2012.

[16] N. Niguchi and K. Hirata, "Torque ripple analysis of a magnetic-geared motor," in *2012 XXth International Conference on Electrical Machines (ICEM)*, pp. 789-794, 2012.

[17] N. Niguchi, K. Hirata, A. Zaini, and S. Nagai, "Proposal of an axial-type magnetic-geared motor," in *2012 XXth International Conference on Electrical Machines (ICEM)*, pp. 738-743, 2012.

[18] E. Morimoto, K. Hirata, N. Niguchi, and Y. Ohno, "Design and analysis of magnetic-geared motor with field windings," *IEEE Trans. Magn.*, Vol. 50, No. 11, Nov. 2014.

[19] N. Niguchi and K. Hirata, "Magnetic-geared motors with high transmission torque density," *COMPEL - The Int. J. Comput. Mathematics in Electr. Electron. Eng.*, Vol. 34, pp. 428-438, 2015.

[20] H. Shi, N. Niguchi, and K. Hirata, "Analytical calculation of air gap magnetic field distribution in vernier motor," in *2017 IEEE 12th International Conference on Power Electronics and Drive Systems (PEDS)*, pp. 247-251, 2017.

[21] H. Shi, N. Niguchi, and K. Hirata, "Analytical calculation of air gap magnetic flux density distribution in magnetic geared motor," in *TENCON 2018 - 2018 IEEE Region 10 Conference*, pp. 0767-0771, 2018.

[22] F. W. Carter, "The magnetic field of the dynamo-electric machine," *J. Inst. Electr. Engineers*, Vol. 64, pp. 1115-1138, Feb. 1926.

[23] Z. Q. Zhu, D. Howe, E. Bolte, and B. Ackermann, "Instantaneous magnetic field distribution in brushless permanent magnet DC motors. I. Open-circuit field," *IEEE Trans. Magn.*, Vol. 29, No. 1, pp. 124-135, Jan. 1993.

Hyoseok Shi received his B.S. and M.S. degrees from Kwangwoon University, Seoul, Korea, in 2010 and 2012, respectively. He is presently working towards his Ph.D. degree in the Department of Adaptive Machine Systems, Graduate School of Engineering, Osaka University, Suita, Japan. His current research includes electrical machines with magnetic gears.

Noboru Niguchi received his B.S., M.S. and Ph.D. degrees from Osaka University, Suita, Japan, in 1998, 2000 and 2011, respectively. He is presently working as an Assistant Professor in the Department of Adaptive Machine Systems, Graduate School of Engineering, Osaka University. His current research interests include electrical machines.

Katsuhiro Hirata received his B.S. degree from Osaka University, Suita, Japan, in 1982; and his Ph.D. degree from Doshisha University, Kyoto, Japan, in 1996. He was a researcher at the R&D Lab, Matsushita Electric Works Ltd. from 1982 to 2005. He joined Osaka University in 2005. He is presently working as a Professor in the Department of Adaptive Machine Systems, Graduate School of Engineering, Osaka University. His current research interests include electromagnetic applied actuators and sensors. He has received a Ministry Award of Education, Science & Technology (Ministry of Education, Culture, Sports, Science and Technology of Japan) in 2003, and is an IEEE member. He received an OHM Technology Award (Promotion Foundation for Electrical Science and Engineering) in 2004. He received an Advanced Technology Award and a Paper Award (IEEJ) in 2007 and 2009, respectively.